International Journal of Nanomedicine

Dovepress
open access to scientific and medical research

Open Access Full Text Article

ORIGINAL RESEARCH

Treatment of Parkinson's disease: nanostructured sol–gel silica–dopamine reservoirs for controlled drug release in the central nervous system

This article was published in the following Dove Press journal:
International Journal of Nanomedicine
15 December 2010
Number of times this article has been viewed

Tessy López[1–3]
José L Bata-García[4]
Dulce Esquivel[5,2]
Emma Ortiz-Islas[2]
Richard Gonzalez[3]
Jorge Ascencio[6]
Patricia Quintana[7]
Gerko Oskam[7]
Fernando J Álvarez-Cervera[4]
Francisco J Heredia-López[4]
José L Góngora-Alfaro[4]

[1]Departamento de Atención a la Salud, UAM-Xochimilco. Calzada del Hueso, Coyoacán, México; [2]Laboratorio de Nanotecnología. Instituto Nacional de Neurología y Neurocirugía MVS, Tlalpan, México; [3]Departamento de Química e Ingeniería Biomolecular, Universidad de Tulane, New Orleans, USA; [4]Departamento de Neurociencias, Centro de Investigaciones Regionales "Dr Hideyo Noguchi", Universidad Autónoma de Yucatán, Mérida, Yucatán; [5]Universidad de Guanajuato, Centro de Investigaciones en Química Inorgánica, Noria Alta Guanajuato; [6]Instituto de Ciencias Físicas-UNAM, Cuernavaca; [7]Departamento de Física Aplicada, CINVESTAV-IPN, Mérida, Yucatán, México

Correspondence: Tessy López
Laboratorio de Nanotecnología. Instituto Nacional de Neurología y Neurocirugía "MVS". Insurgentes Sur 3877, Col. la Fama, Tlalpan 14269, México, DF
Tel +01 525 606 3822 ext 5034
Fax +01 525 524 0808
Email tessy3@prodigy.net.mx

Introduction: We have evaluated the use of silica–dopamine reservoirs synthesized by the sol–gel approach with the aim of using them in the treatment of Parkinson's disease, specifically as a device for the controlled release of dopamine in the striatum. Theoretical calculations illustrate that dopamine is expected to assume a planar structure and exhibit weak interactions with the silica surface.

Methods: Several samples were prepared by varying the wt% of dopamine added during the hydrolysis of tetraethyl orthosilicate. The silica–dopamine reservoirs were characterized by N_2 adsorption, scanning and transmission electron microscopy, and Fourier transform infrared spectroscopy. The in vitro release profiles were determined using ultraviolet visible absorbance spectroscopy. The textural analyses showed a maximum value for the surface area of 620 m^2/g nanostructured silica materials. The stability of dopamine in the silica network was confirmed by infrared and ^{13}C-nuclear magnetic resonance spectroscopy. The reservoirs were evaluated by means of apomorphine-induced rotation behavior in hemiparkisonian rats.

Results: The in vitro dopamine delivery profiles indicate two regimes of release, a fast and sustained dopamine delivery was observed up to 24 hours, and after this time the rate of delivery became constant. Histologic analysis of formalin-fixed brains performed 24–32 weeks after reservoir implantation revealed that silica–dopamine implants had a reddish-brown color, suggesting the presence of oxidized dopamine, likely caused by the fixation procedure, while implants without dopamine were always translucent.

Conclusion: The major finding of the study was that intrastriatal silica–dopamine implants reversed the rotational asymmetry induced by apomorphine, a dopamine agonist, in hemiparkinsonian rats. No dyskinesias or other motor abnormalities were observed in animals implanted with silica or silica–dopamine.

Keywords: Parkinson's disease, silica–dopamine, controlled drug release, central nervous system, reservoirs

Introduction

Parkinson's disease is an illness of the central nervous system that leads to severe impairment of motor skills and difficulty in controlling body movements. The characteristic symptoms are tremor, rigidity, slowed body movements (bradykinesia), unstable posture, and difficulty in walking.[1–3] Smoking, alcohol, coffee, cocaine, amphetamine, and opiate abuse have all been shown to have somewhat of a preventative effect in the onset of Parkinson's disease.[4–6] Parkinson's disease is characterized by a progressive degeneration of dopaminergic neurons in the substantia nigra pars compacta region of the brain, leading to a massive loss of dopamine in the striatum.[7] To date, Parkinson's

disease remains an incurable disease. Because dopamine does not cross the blood–brain barrier, it cannot be used as replacement therapy in patients with Parkinson's disease.[8] Instead, its immediate precursor, L-hydroxyphenylalanine (L-dopa), has good brain penetration, rendering it the most efficacious treatment. However, during long-term use of L-dopa, many patients with Parkinson's disease develop motor response fluctuations that, in many cases, force treatment discontinuation (eg, wearing off, on-off fluctuations, night-time deterioration, early morning worsening, and dyskinesias).[9,10] These side effects have been linked to fluctuations of striatal dopamine levels during intermittent L-dopa therapy, and some success in reducing them has been obtained with the use of slow-release L-dopa formulations.[11] The currently available pharmacologic and nonpharmacologic treatments are capable of offering only symptomatic relief for patients.[12]

One way to combat this problem is to develop controlled drug-release systems for reducing drug dosage and to make the drug available at the target sites. A large variety of such systems have been developed and used, including liposomes, micelles, dendrimers, and copolymers.[13] Oxide nanomaterials have recently attracted attention as potential drug-release carriers due to their versatile physiochemical properties, including easy synthesis, tailorable surface charge density and facile surface functionalization, good biocompatibility, and low cytoxicity.[14–16] In particular, silica-based materials have attracted interest[17–20] due to their excellent biocompatibility and because they can be engineered into a variety of nanoshapes. Furthermore, the rate of bioerosion can be tuned by changes in the synthesis or postprocessing conditions.[21] Therefore, sol–gel-derived silica xerogels have been studied as carrier materials for the controlled release of various drugs, proteins, and peptides.[22–24] Using this material, we previously showed an antiepileptic effect in rats implanted with a valproic acid-loaded nanosilica reservoir in the amygdala.[25] Recently, we described the stabilization of dopamine in a nanosilica sol–gel matrix to be used as a controlled drug-release system.[26]

In this work, dopamine was incorporated into a silica network structure using the sol–gel method. The reservoirs were characterized by a variety of methods in order to evaluate the stability of the dopamine molecule in the nanomaterial, as well as the interactions between the drug and the silica network. The aim of this work was to obtain a drug-release device for use as an intracranial implant, specifically in damaged regions. For this purpose, we evaluated the therapeutic efficacy of striatal dopamine release from a silica reservoir in hemiparkinsonian rats by studying the circling behavior induced by apomorphine before and after the implantation, in a similar fashion to the experimental design used in studies of cell transplants.[27]

Methods

Theoretical analysis

Calculations were performed using local density approximation. Density functional theory was employed using DMo13 high precision software. The models were established and then geometrically optimized. This was followed by a calculation of the single point-to-point energy in order to identify the most stable energy state, the electrostatic potential associated with the molecule, and the characteristic Fukui potentials, as previously reported.[28]

Preparation of silica–dopamine

Four different samples of silica, containing 9.09, 19.2, 33.33 and 42.85 wt% of dopamine, were prepared by the sol–gel process. In general terms, the following procedure was carried out for each sample: 2, 5, 10, and 15 g of dopamine (99%; Sigma-Aldrich, St. Louis, MO) were dissolved in 239 mL of water. Afterwards, 68.74 g of tetraethoxysilane (Sigma-Aldrich) were added dropwise to this solution. The resulting solution was continuously stirred at room temperature until gel formation, and the obtained gel was dried at 80°C. The drying process was carried out in nitrogen atmosphere in order to avoid the oxidation of dopamine.

Characterization

^{13}C-nuclear magnetic resonance spectroscopy

The spectra were obtained using a Varian Gemoni 200 spectrometer (Varian, Palo Alto, CA).

Fourier transform infrared spectroscopy

Silica–dopamine samples were mixed with KBr (5 wt%) and pressed into transparent wafers. Fourier transform infrared spectra were recorded using a Perkin-Elmer 1600 spectrophotometer (Perkin-Elmer, Shelton, CT) in the 4000–400 cm^{-1} range, and 32 scans were run for each measurement.

Textural properties

Adsorption-desorption measurements were performed on an ASAP 2010 Micromeritic apparatus (Micrometrics, Atlanta, GA). The samples were previously degassed at room temperature and 10^{-3} Torr for several hours. Adsorption-desorption measurements were then performed at liquid nitrogen temperature (77 K) and 10^{-6} Torr vacuum pressure. Successive known volumes of N_2 gas were admitted to the

adsorbent at programmed intervals and equilibrium pressure was measured. Similarly, desorption isotherms were obtained by measuring the quantities of gas removed from the sample as the relative pressure was lowered. Analysis of the surface area of the samples was done according to the most widely used procedure of the Brunauer–Emmett–Teller (BET) method. Pore size distributions and adsorbed volume were calculated using the Barrett, Joyner, and Halenda (BJH) theory and desorption branches, respectively.

Transmission electron microscopy

Particle size was measured using conventional transmission electron microscopy (TEM, Zeiss EM910; Carl Zeiss, Oberkochen, Germany), operated at 100 kV, with a side entry goniometer and 0.4 nm point-to-point resolution, and attached to a CCD camera (MegaVision, Santa Barbara, CA).

In vitro dopamine release

Dopamine release measurements were carried out by means of ultraviolet-visible spectrophotometry utilizing a Varian CARY 1 instrument (Varian). The absorbance was monitored at $\lambda = 280$ nm. In order to avoid dopamine oxidation, it was necessary to use a nitrogen atmosphere and an amber recipient, as shown in Figure 1. Each sample was compressed into a tablet of 19.8, 12.7, 18.4, and 8.3 mg for each sample in increasing order of dopamine content and immersed in 200 mL of deionized water. At predetermined time intervals, 4 mL of the solution was withdrawn, and the ultraviolet-visible absorbance spectrum was measured. After each measurement, the aliquot was returned to the original solution. A calibration curve of absorbance versus dopamine concentration was used to determine the concentration of released dopamine, as shown in Figure 2.

In vivo dopamine studies

Experiments were conducted on 17 male Wistar rats bred in our facilities. The initial average weight was 229 ± 9 g (range 238–268 g), which increased to 415 ± 10 g (range 345–495 g) at the end of the experimental period. Animals were individually housed in acrylic cages at constant room temperature (23 ± 1°C) and maintained on a 12:12 hour light/dark cycle (lights on at 7am) throughout. Food and water were available ad libitum. All efforts were made to minimize animal discomfort according to the recommendations of the Guide for the Care and Use of Laboratory Animals (National Research Council of USA, 1996). This study was approved by the Institutional Bioethics Committee of the CIR-UADY.

Following an intraperitoneal dose of desipramine 25 mg/kg to protect the central noradrenergic neurons, rats were anesthetized with intraperitoneal sodium pentobarbital 45 mg/kg and placed in a stereotaxic frame (Stöelting, Wood Dale, IL) with the incisor bar set at 3.3 mm below the interaural line. A single dose of 6-hydroxydopamine 9 µg/3 µL, (Sigma-Aldrich) was manually injected in small

Figure 1 Set-up for the study of dopamine release from silica reservoirs. The experiments were performed in amber glass bottles and under nitrogen atmosphere in order to prevent dopamine oxidation.

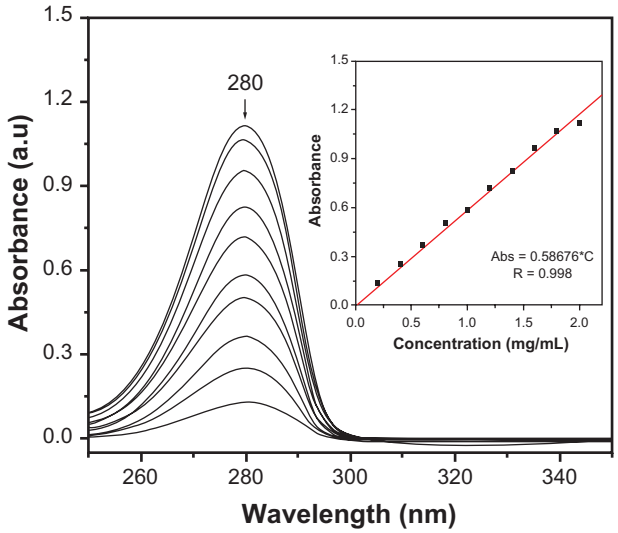

Figure 2 Absorbance spectra of standard solutions as a function of dopamine concentration. The inset shows the calibration curve used to determine the dopamine release kinetics from reservoirs.

steps (at approximately 0.2 µL/min) into the right substantia nigra pars compacta, at the coordinates *AP*, −5.3 mm from bregma; *L*, −1.8 mm from the midline, and *V*, −7.6 mm from the dura surface.[29] Infusion was made through a 30 gauge needle connected with a polyethylene catheter (PE10) to a 10 µL microsyringe (Hamilton, Reno, NV). Upon completion of the injection, the needle was left in place for an additional minute before withdrawal.

In order to select those animals bearing successful striatal dopamine denervation (>90%) they were tested for apomorphine-induced rotation two weeks after lesion surgery. The rotational test was done by placing the rats in hemispheric bowls (41 cm diameter), secured to a harness, and connected with a steel wire to an automated rotometer.[30] A subcutaneous dose of apomorphine 0.25 mg/kg was then applied, and the rotational behavior counted during 90 minutes. Only rats performing a minimum of 100 complete turns (360°) contralateral to the lesioned side during the 90-minute test were used in the experiments (Figure 3).

The selected rats were divided in three groups: rats without implant surgery (lesion-only group), rats implanted with empty silica reservoirs (silica group), and rats implanted with reservoirs impregnated with dopamine (silica–dopamine group). The second rotational test was performed in the same way 24 weeks after the lesion, which corresponded to 16 weeks after surgical implantation of the nanostructured reservoirs in the striatum (Figure 3). This last test allowed assessment of whether the rats with silica–dopamine implants experienced the expected reduced behavioral asymmetry in comparison with lesion-only animals or those implanted with the empty silica reservoir. The reduction or increase in the number of contralateral turns (CLT) between the first (two weeks) and the second (24 weeks) rotational tests after the 6-hydroxydopamine lesion was measured as the percent change (ΔCLT%), according to the formula:

$$\Delta CLT\% = (CLT\ 24\ weeks - CLT\ 2\ weeks)/(CLT\ 2\ weeks) \times 100.$$

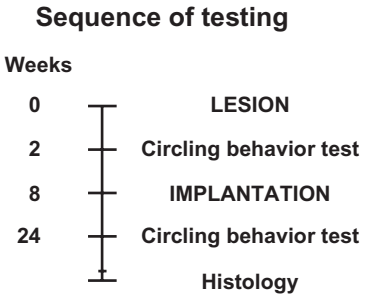

Figure 3 Experimental design. In all experimental groups, the circling behavior tests were performed two and 24 weeks after the unilateral nigral 6-hydroxydopamine lesion. In two groups of lesioned rats, a silica nanostructured material, with or without dopamine, was surgically implanted in the dopamine denervated striatum during the eighth week after the lesion.

Surgical implantation

Surgical implantation of silica reservoirs was done during the eighth week after the 6-hydroxydopamine lesion. Rats were anesthetized and placed in a stereotaxic frame as before. About 1.5 mg of the nanosilicon powder, either silica or silica–dopamine, was packed into the lumen of a 17 gauge stainless steel unbeveled rachidian needle. The resulting cylinders were approximately 1 mm in diameter and 2 mm in length. One silica cylinder with or without dopamine was surgically implanted into the right striatum by gently pushing the nanosilica material with a steel piston, such that the lower end of the implanted cylinder would be positioned at the following coordinates: *AP*, 1.0 mm from bregma; *L*, −3.3 mm from the midline, and *V*, −6.5 mm from the dura surface.[31] After recovering from the surgery, rats remained in their home cages with food and water ad libitum for one month before starting the behavioral tests.

Histology

Once the behavioral tests had been completed, rats were anesthetized and perfused through the ascending aorta with phosphate-buffered saline (0.1 M, pH 7.4) followed by ice-cold paraformaldehyde 4% in phosphate-buffered saline. This occurred between 16 and 28 weeks after surgical implantation of the silica. The brains were removed, postfixed for two hours in the same fixative at room temperature, and placed overnight in phosphate-buffered saline with 15% sucrose at 4°C. Serial coronal sections (50 µm) of the striatum were cut using a vibroslicer (Vibratome, Bannockburn, IL) and sequentially placed in multiwells with phosphate-buffered saline. Freshly cut sections of striatum at the level of the implants (silica or silica–dopamine) were photographed with a digital camera (Olympus DP11) adapted to a stereoscopic microscope Olympus SZ11 (Olympus, Tokyo, Japan).

Data analysis

In compliance with international policies for the use of animals in neuroscience research, the number of rats used in this study was kept to the minimum necessary to obtain statistically significant results. Data are expressed as means ± standard error of the mean. The time-courses of circling behavior during weeks 2 and 24 were analyzed using two-way analysis of variance, and the cumulative rotation values were com-

pared using the paired Student's *t*-test. The percent change between the first and second rotation tests did not follow a normal distribution, and hence data were analyzed using the Kruskal–Wallis test, followed by Dunn's post hoc multiple comparison test. The significance level was set at 0.05. All statistical analyses were performed using GraphPad Prism version 4 (GraphPad Software Inc, La Jolla, CA).

Results and discussion

In Figure 4, the structural analysis of a dopamine molecule is represented. Possible modifications in its electronic structure as a result of the presence of H atoms can be observed following the approach of a nanostructured silica unit. This was used to identify the electrophilic and nucleophilic sites. As a result of these calculations (Figure 4) it is possible to understand that the most stable configuration tends to place the ring of the molecule in a planar structure, enabling equivalent interactions with any of its atoms as a function of structure and electron affinity. It is precisely this electrostatic potential that shows how the sites in close proximity to the nitrogen atoms and those that surround the benzene ring in the direction of the oxygen atoms clearly define the polarity of the molecule.[31,32]

The isosurface of the highest occupied molecular orbital of the molecule is centered on the ring, leaving only a small residue outside. This phenomenon modifies the application of dopamine, because the associated chemical potential is totally different. The evident effects on the silica–dopamine system can be seen in the location of the electrophilic sites [f(−)] and nucleophilic sites [f(+)] that define the tendency for reactions. Figure 5 shows the location of the sites for

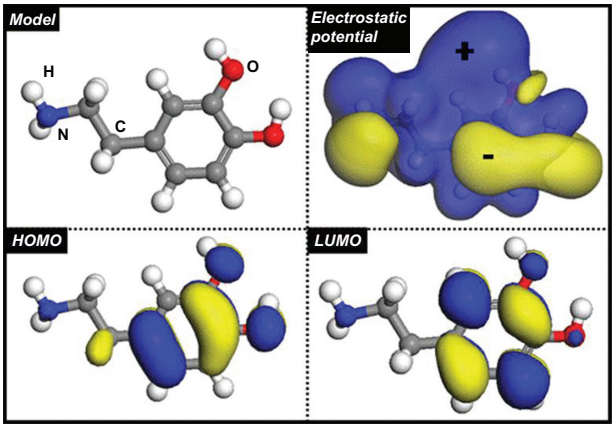

Figure 4 Atomic and electron structure of dopamine calculated by quantum mechanical methods, also illustrating the highest occupied molecular orbital and lowest unoccupied molecular orbital spatial distribution.

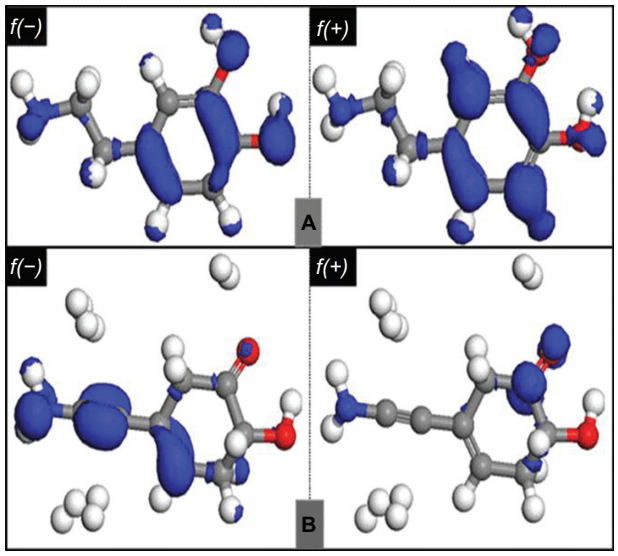

Figure 5 Calculated atomic and electron structure of dopamine **A**) Neutral molecule and **B**) in the presence of hydrogen atoms (see text for details).

two conditions, a) when the dopamine is considered as a neutral molecule, and b) in the presence of hydrogen atoms, whereby the distribution of the sites is strongly modified in the presence of hydrogen. It is clear that the modified system should be more reactive and thus becomes the preferred reaction pathway in interactions with the silica reservoir. This behavior causes the functional groups of dopamine (NH and OH) to interact efficiently with the receptors of the sol–gel silica matrix.

In order to evaluate the interaction modes in the molecule without previous perturbation, a geometric optimization calculation of one dopamine molecule in the proximity of a nanostructured silica segment was performed. The most feasible interactions stabilized the dopamine in the hydroxylated sol–gel silica. This process is illustrated in Figure 6. The calculations were performed using two different orientations for the initial step: a dopamine molecule above the nanostructured silica reservoir (Figure 6a), and a dopamine molecule besides the nanostructured silica reservoir (Figure 6b). It was found that dopamine is attracted to the silica in a coplanar form. Nevertheless, the minimum energy was obtained when the molecule was linked to the silica network via the silanol groups and the amine, carboxyl, and hydroxyl groups of the drug, which are characterized by noncovalent and weak interactions. Hence, dopamine molecules were completely stable in the silica nanomaterial[26] (a white material was obtained), and this is in agreement with the ^{13}C-nuclear magnetic resonance spectroscopy analysis, which indicated that drug degradation was not observed, as shown in Figure 7. Likewise, the two coordination types between the drug and silica also show

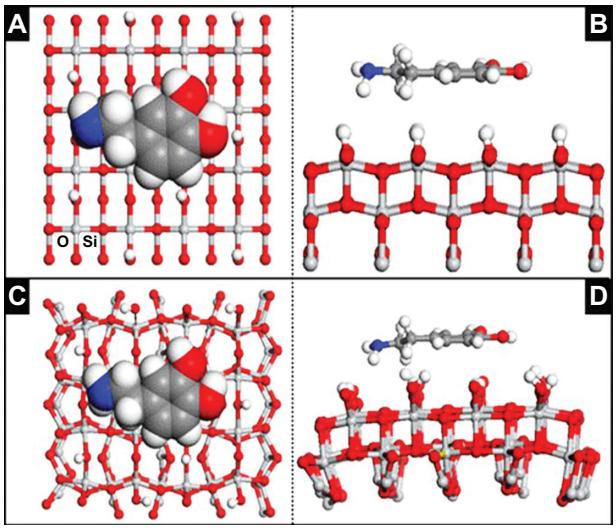

Figure 6 Calculated structure of a silica net segment and geometric optimization of the framework with one dopamine molecule: **A)** original configuration, **B)** relaxed structure, **C)** top view of the deformation of the silica framework with dopamine, and **D)** side view.

hydrogen bonds. The presence of OH groups generates a passive section in the inorganic matrix and a deformation of the network is observed (Figures 6c and 6d). The hydrogen bridges are somewhat stronger than the other interactions, although this does not impede release of the drug in an aqueous medium, such as cerebrospinal fluid. These results illustrate that the silica–dopamine system shows promising characteristics for brain drug-release systems.

Textural properties

The N_2 adsorption-desorption isotherms of the four samples are shown in Figure 8. Approximately 80%–90% of the total uptake at 0.7 P/P_0 takes place within 0.7–1.0 P/P_0. The isotherms exhibit a steep slope and hysteresis at relative pressures higher than 0.7, which may be associated with capillary condensation in larger mesopores, and the isotherms can be classified as Type IV according to International Union of Pure and Applied Chemistry definitions.[33] The hysteresis loop observed for 9.09 wt% and 19.2 wt% samples indicates a textural mesoporosity in the particle aggregates, thus evidencing the presence of external surfaces between the particles. However, the hysteresis loop observed for the 33.33 wt% and 42.85 wt% materials indicates the presence of spaces between parallel sheet structures. In all samples the N_2 uptake at higher P/P_0 values is due to the dominating presence of mesopores. The mesoporosity of silica obtained from the sol–gel process through hydrolysis of silicon alkoxide in the presence of an organic additive has been attributed to electrostatic interaction between the silica sol particles and the organic additive. We consider that the same mechanism prevails in the formation of mesoporous silica in the silica–dopamine system. The structure-directing effect of dopamine in the silica gel complex is that of cooperative organization between the organic and inorganic groups. It may be noted here that the sol–gel process produces silica particles in the nanometer length range; however, when dopamine is added at high concentration, the nanomaterial structures constitute parallel sheets.

The pore sizes of the samples were obtained using the BJH theory,[34] which takes into account the formation of a liquid-like adsorbate layer on the pore walls which precedes capillary condensation or follows capillary evaporation. In order to measure the thickness of the adsorbate layer, t, on the adsorbate relative pressure, x (x = P/P_0, where P is the adsorbate pressure and P_0 is the adsorbate vapor pressure at the measuring temperature), a "universal" dependence, t(x), is used, which is believed to apply for diverse surface types of porous solids. The pore size distribution using the desorption branch of N_2 isotherms are shown in Figure 9. The 19.2 wt% sample presents a wide pore size distribution, while the rest of the samples present a narrow one.

The BET surface area, volume pore, and average pore size are summarized in Table 1. The BET surface areas were calculated from the BET plots at the P/P_0 range of 0–0.4. From these data, we can deduce that the sample with 19.22 wt% of dopamine has the largest surface area of 620 m^2/g. At either higher or lower dopamine concentrations, the surface area of the reservoir materials is approximately 100 m^2/g. In general, the average pore size is between 100 and 200 Å for all samples, corresponding to mesoporous materials. The corresponding mesopore volume for all samples is approximately 0.4 cc/g (see Table 1).

Fourier transform infrared spectroscopy

The Fourier transform infrared spectra of dopamine and silica–dopamine samples are shown in Figures 10 and 11, respectively. A wide band at low energy enclosing three important peaks is observed for dopamine, as shown in Figure 9. The peaks at 3350 cm^{-1}, 3205 cm^{-1}, and 3034 cm^{-1} are assigned to stretching vibrations of the OH, CN, and NH groups of dopamine, respectively. Other small peaks are observed in the range of 2778–2170 cm^{-1}, corresponding to different CH vibrations of either aryl or aliphatic CH bonds. At higher energies, important bands are observed at 1494 cm^{-1} and at 1252 cm^{-1}, corresponding to the bending vibration of CH and the aryl oxygen stretching vibration, respectively. The peak at 1342 cm^{-1} is attributed to the OH groups of the dopamine molecule.

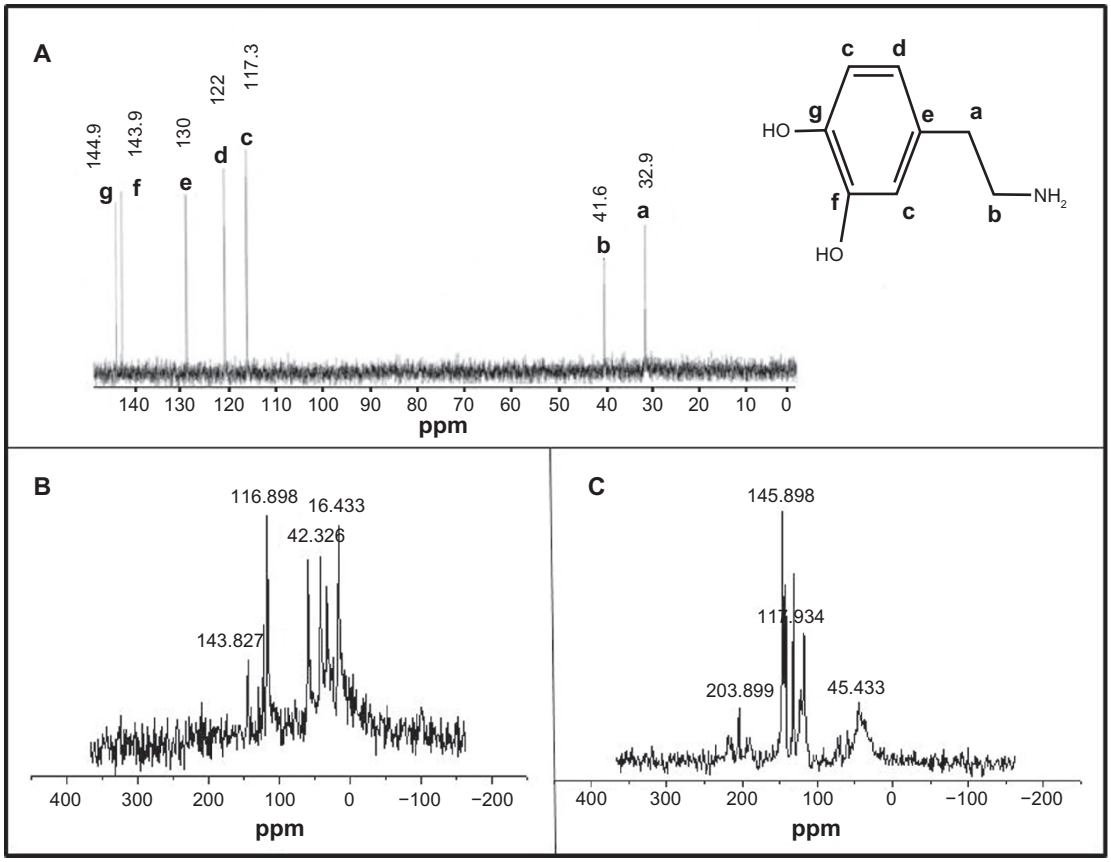

Figure 7 ^{13}C-magnetic nuclear resonance spectra of **A)** pure dopamine, a to g signals correspond to different carbon atoms of dopamine. **B)** These signals were observed in the silica–dopamine sample. **C)** Signals of oxidized dopamine in silica materials. The signal at around 45 ppm indicates that dopamine is polymerized.

Figure 11 shows the spectra corresponding to dopamine loaded into the silica network, and it can be seen that the peaks corresponding to the OH, CN, and NH vibrations of dopamine become better defined and stronger with increasing dopamine concentrations. However, the peaks are shifted to slightly higher energies, which is attributed to weak interactions, such as Van der Waals forces and hydrogen bridges between dopamine and the hydroxyl groups of the silica matrix.[26] The peaks corresponding to the bending vibration of CH groups and the stretching vibration of the aryl oxygen of dopamine

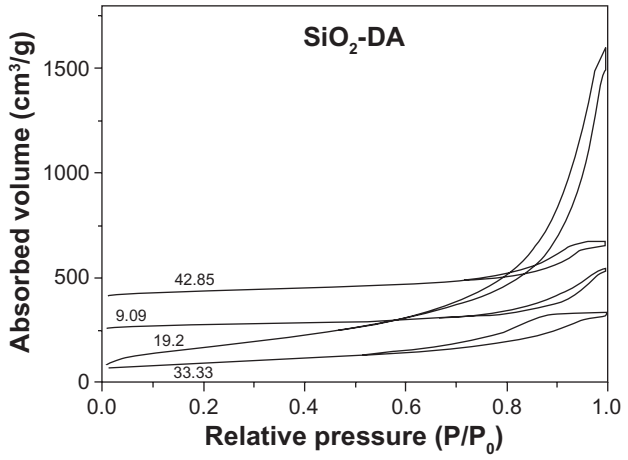

Figure 8 N_2 adsorption-desorption isotherms of silica reservoirs with different dopamine concentrations.

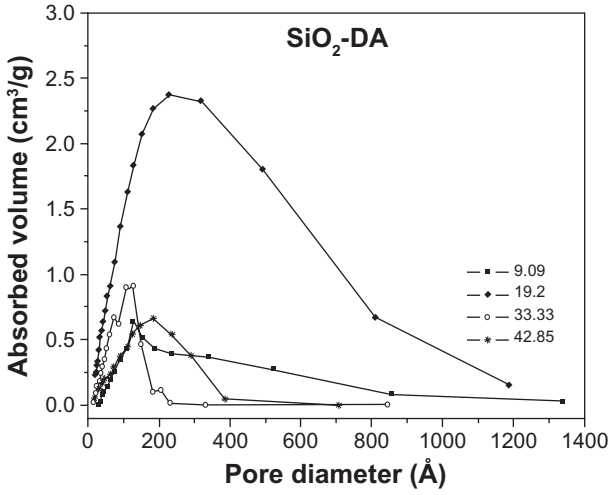

Figure 9 Pore size distributions for the silica–dopamine samples studied.

Table 1 BET_{AREA}, average pore diameter, and pore volume of different silica–dopamine materials

Sample	BET_{AREA} m^2/g	Pore diameter (Å)	Pore volume (cc/g)
SiO_2-DA 9.09	100	170	0.4291
SiO_2-DA 19.2	620	147	2.2866
SiO_2-DA 33.33	172	101	0.4374
SiO_2-DA 42.85	136	124	0.4261

Abbreviations: BET_{AREA}, area calculated by the Brunauer–Emmett–Teller method; SiO_2-DA, silica–dopamine.

were also observed at somewhat higher energies. These results suggest that dopamine was successfully loaded in the silica sol–gel matrix and that the drug is stable.

The most important bands corresponding to silica structures were also observed in the spectrum shown in Figure 11. A band centered at 3385 cm^{-1} is attributed to the OH stretching vibrations of silanol groups. The band localized at 1632 cm^{-1} is related to adsorbed water and is generated by symmetric stretching vibrations of the hydrogen atoms with the oxygen atom. A high intensity band at 1092 cm^{-1} accompanied by a shoulder at 1210 cm^{-1} are due to asymmetric stretching vibrations of ≡ Si-O-Si ≡. The band at 956 cm^{-1} is due to the silanol groups. Another band present at 805 cm^{-1} is due to asymmetric flexion of the ≡Si-O bonds.[35] Finally, the band at 566 cm^{-1} appears to be due to bending vibrations of O-Si-O.

Transmission electron microscopy

Figure 12 shows TEM images of the silica–dopamine materials with varying concentrations of dopamine. In general terms, all samples show a morphology consisting of aggregated particles, with sizes depending on the dopamine concentration. For the sample with 9.09 wt% of dopamine, the particle size was found to be 50–150 nm. Most likely these particles consist of aggregated nanoparticles, thus accounting for the presence of mesopores with an average size of about 10 nm. For the sample of silica containing

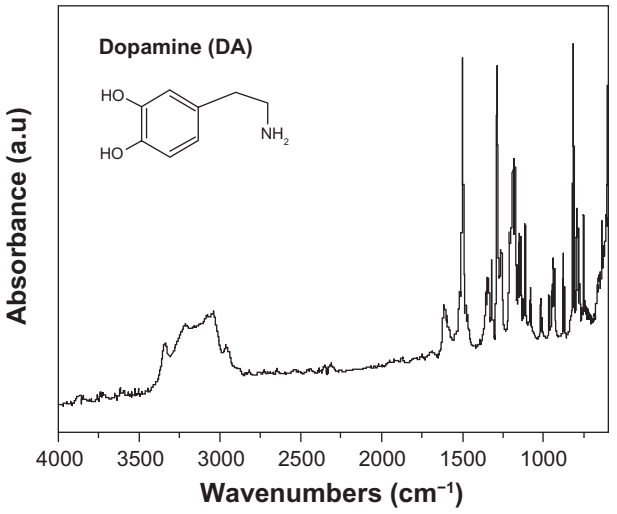

Figure 10 Fourier transform infrared spectrum of dopamine.

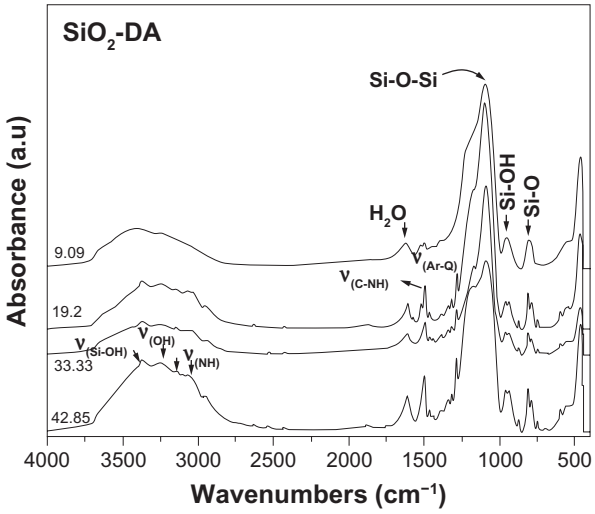

Figure 11 Fourier transform infrared spectra of dopamine-loaded sol–gel silica.

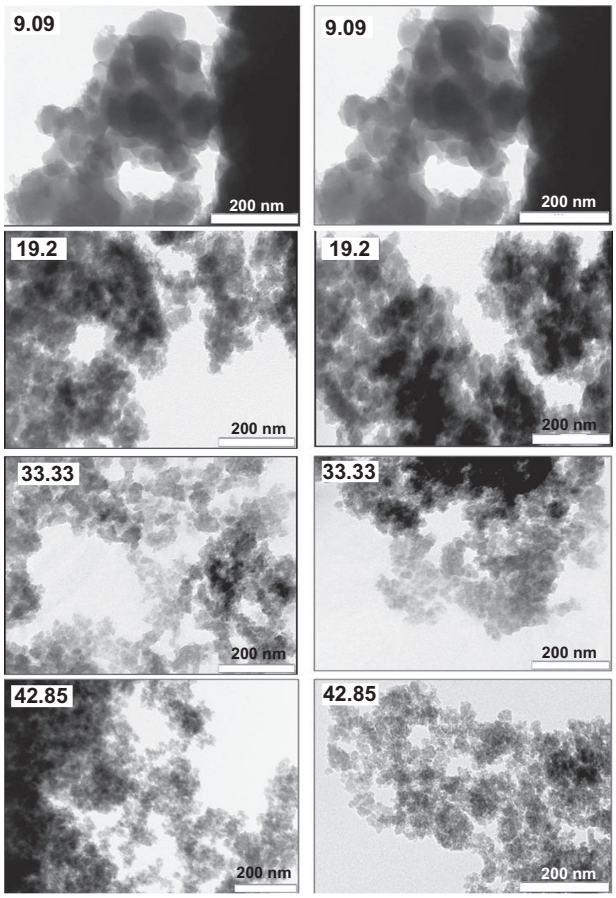

Figure 12 Transmission electron microscopy images of the different silica–dopamine materials at different magnifications, showing nanoparticle aggregates.

dopamine 19.2 wt%, the average particle size was around 40 nm, while most of the particles in the sample with 33.33 dopamine wt% had a size of approximately 25 nm. The sample with the highest content of dopamine at 42.85 wt% had a particle size of around 15 nm. These results indicate that the presence of dopamine during the preparation of the silica matrix strongly affects the morphology of the reservoir material. Interestingly, the dependence of the particle size on the dopamine concentration appears much more pronounced than that of the average size of pores.

X-ray diffraction

The X-ray diffraction patterns of silica–dopamine materials are shown in Figure 13, in which an undefined broad band characteristic of amorphous silica is shown. Diffraction peaks corresponding to dopamine were not seen, thus indicating that dopamine was highly dispersed into the amorphous network of silica.

In vitro dopamine release kinetics

The release kinetic profiles of dopamine from the silica–dopamine reservoir materials were studied for 100 hours using ultraviolet visible spectrophotometry, and the results are shown in Figures 14 and 15. The kinetic profiles were obtained by quantifying the accumulated amount of dopamine released as a function of time, and are shown in Figure 14, and correspond to the 9.09 wt% silica–dopamine sample. From Figure 15 it can be observed that, in all cases, the silica–dopamine reservoirs show a sharp initial burst of dopamine release during the first 24 hours. This is attributed to the immediate dissolution and release of the portion of the drug located on and near the surface of the disks. The amount of released dopamine can be compared with the amount of incorporated dopamine. For the 9.09 wt% sample, 1.68 mg of dopamine were originally present in the reservoir, and essentially 70% of this was released at 24 hours. This can be related to the morphology observed with TEM, which showed relatively large particle sizes, suggesting the presence of macropores. It appears that, in this case, the majority of the dopamine was incorporated in macropores, allowing fast release upon immersion in a solution. For the 19.2 wt% sample, about 2.45 mg of dopamine were incorporated, and about 20% was released within the first 24 hours. Further release of the remaining dopamine appears to be very slow, as evidenced by the

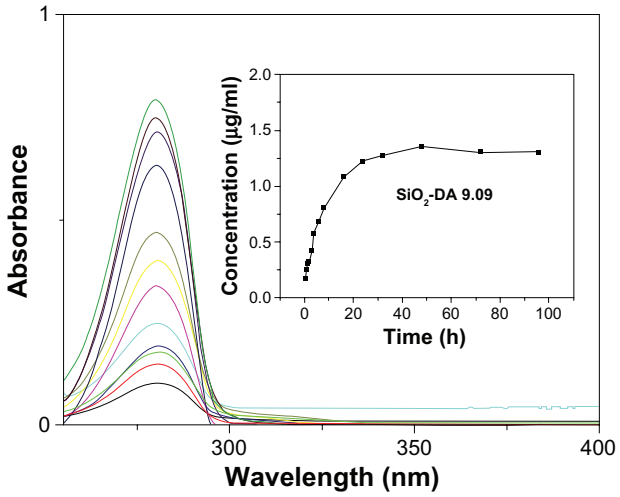

Figure 14 Cumulative dopamine concentration as a function of release time for the 9.09 dopamine-silica sample, illustrating the two-stage release kinetics.

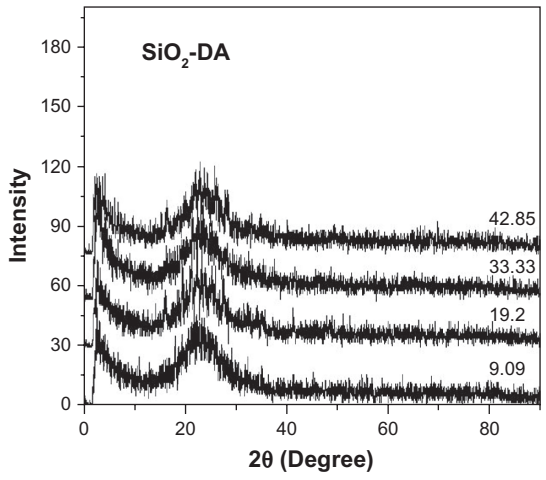

Figure 13 X-ray diffractograms of the silica–dopamine materials. The broad peak indicates no crystalline silica materials.

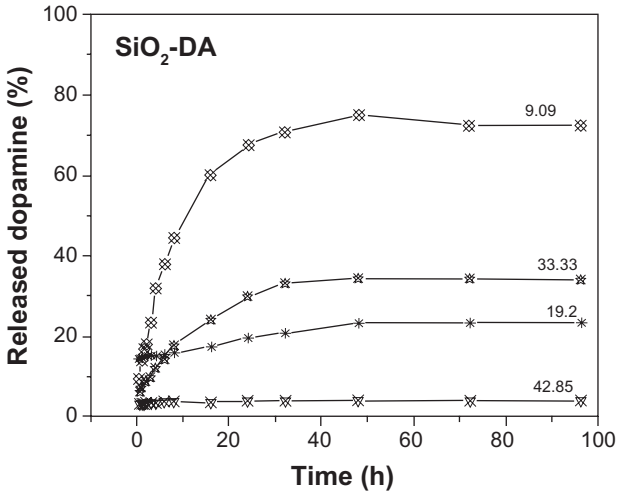

Figure 15 Dopamine release profiles for the four silica–dopamine reservoirs.

essentially time-independent dopamine concentration in the solution. For the sample with 33.33 wt% dopamine, about 50% of it was released within the first 24 hours, whereas for the 42.85 wt% sample about 4.5% was released during the first 24 hours. Hence, it can be concluded that the release kinetics depend on the morphology and composition of the silica–dopamine reservoir material, the general trend being that initially less dopamine is released with smaller particle size, as observed with TEM. Also, the efficient initial release of dopamine from the samples with dopamine 9.09 wt% and 19.2 wt% can be related to their larger average pore sizes compared with those for the materials with higher dopamine concentrations. The very slow release of dopamine after the initial hours may be related to a relatively strong interaction between the drug and the mesoporous silica through a hydrogen bond due to the affinity between the functional amine and hydroxyl groups of dopamine and the silanol groups present on the sol–gel silica, as indicated by the relatively polar hydrophilic character of the drug. These results are in agreement with those obtained from the theoretic calculations, although the release rate cannot be adequately predicted. The strength of interaction between dopamine and the silica network is expected to depend on the pH of the solution, indicating that the in vivo release rate will be conditioned by the properties of the local environment around the reservoir.

In vivo dopamine studies

Rats with lesions induced by 6-hydroxydopamine performed tight, full rotations toward the nonlesioned side (contralateral turns) after apomorphine challenge. Two weeks after the lesion, 17 animals met the criteria of performing a minimum of 100 contralateral turns in 90 minutes (511 ± 70, range 104–1104).

No dyskinesias or unexpected motor abnormalities were observed in animals implanted with silica or silica–dopamine. Comparisons of circling behavior recorded after the first and second apomorphine challenges showed different time-course profiles in the animals without striatal implants (Figure 16A), in those implanted with an empty silica reservoir (Figure 16C), as well as in those bearing the silica–dopamine complex (Figure 16E).

In the nonimplanted group, the onset of rotations was faster and their duration was longer at 24 weeks than at two weeks after lesion surgery (Figure 16A). The cumulative number of contralateral turns two weeks after the lesion was 341 ± 91, and was significantly increased to 572 ± 26 at 24 weeks after the lesion (Figure 16B).

In animals with the empty silica reservoir, there were no differences in the onset, intensity, or duration of circling recorded 24 weeks after the lesion (16 weeks after implantation) in comparison with those recorded two weeks after the lesion (six weeks before implantation, Figure 16C). The cumulative number of contralateral turns recorded before implantation was 452 ± 60, and this number did not change significantly after implantation (480 ± 92, Figure 16D).

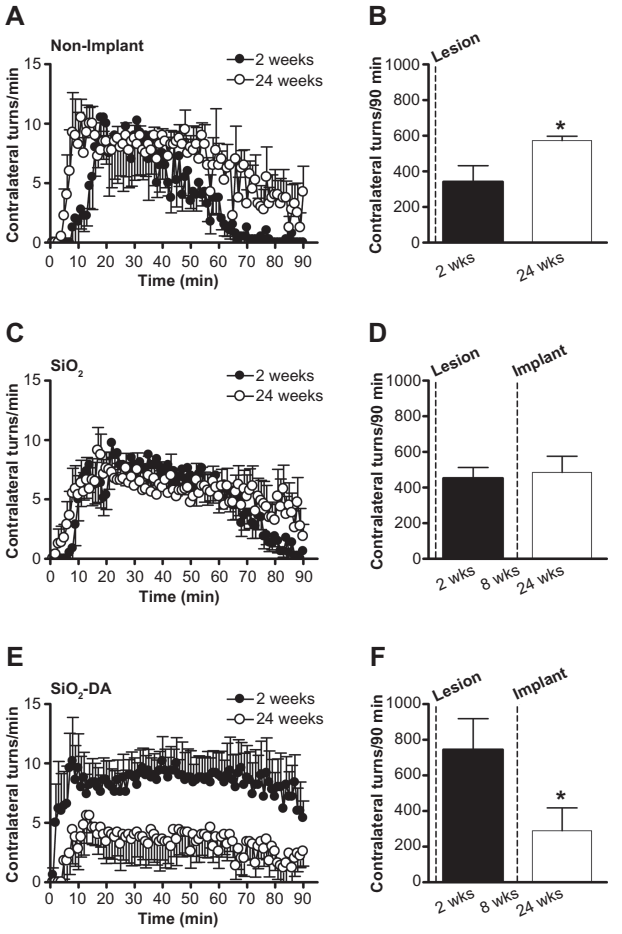

Figure 16 Temporal profile and total number of turns induced by apomorphine in hemiparkinsonian rats. **A**, **C**, and **E** illustrate the time course of contralateral circling after apomorphine challenge (t = 0). **B**, **D**, and **F** show the cumulative number of turns during 90 minutes. **A)** Animals without an implant (n = 4) performed more turns during the evaluation at week 24 than at week 2 after lesion. Two-way analysis of variance revealed a significant effect of week ($F1,540 = 91.4$, $P < 0.0001$) and time ($F89,540 = 5.1$; $P < 0.0001$), but not of the interaction between the two factors ($F89,540 = 0.9$; $P > 0.05$). **B)** Cumulative turns of animals without implant (paired *t*-test, $t[3] = 3.1$, $^*P = 0.027$). **C)** Animals implanted with an empty silica–dopamine reservoir (n = 8) showed no difference in circling behavior between weeks 2 and 24 after lesion. Two-way analysis of variance showed no significant effects of week ($F1.1260 = 3.3$, $P > 0.05$), time ($F89,1260 = 5.0$, $P > 0.05$), or interaction between the two factors ($F89,1260 = 1.0$, $P > 0.05$). **D)** Cumulative turns of animals with silica–dopamine implants (paired *t*-test, $t[7] = 0.3$, $P > 0.05$). **E)** Animals implanted with silica–dopamine (n = 5) performed fewer turns during week 24 than during week 2 after lesion. Two-way analysis of variance revealed a significant effect of week ($F1,720 = 280$; $P < 0.0001$), but not of time ($F89,720 = 0.599$; $P > 0.05$) or interaction between the two factors ($F89,720 = 0.167$; not significant). **F)** Cumulative turns of animals with silica–dopamine implants (paired *t*-test, $t[4] = 2.9$, $^*P = 0.023$).

In animals implanted with silica–dopamine, a significant reduction of circling was observed 24 weeks after the lesion (16 weeks after implantation) in comparison with those recorded two weeks after the lesion (six weeks before implantation, Figure 16E). The cumulative number of contralateral turns recorded before implantation was 744 ± 174, and was significantly reduced to 289 ± 127 at 24 weeks after the lesion (Figure 16F).

When the rotations recorded on the second test were expressed as a percentage of the circling values measured on the first test, it was found that the silica–dopamine group, but not the silica group, had a significant reduction of circling behavior, in comparison with the nonimplanted group (Figure 17).

Consistent with previous studies,[27,36] here we found that unilateral dopamine denervation with 6-hydroxydopamine, a catecholamine selective neurotoxin, caused motor asymmetry in rats, which displayed rotational behavior contralateral to the lesioned side after a challenge with apomorphine, a dopamine agonist. Earlier studies have shown that this effect occurs only in rats bearing a loss of dopaminergic neurons in the substantia nigra pars compacta of at least 90%.[37] Using the tyrosine hydroxylase immunostaining protocol we have previously confirmed that the method of surgical lesion used in the present study produces more than 90% of dopamine denervation in the substantia nigra pars compacta and ipsilateral striatum.[38]

It is important to note that the inhibitory effect of silica–dopamine implants on apomorphine-induced circling was observed 16 weeks after surgery, suggesting that they were still releasing dopamine in the surrounding striatal tissue. Although the residual content of dopamine in the implants was not determined, its possible presence in the reservoirs was suggested by the results of the histologic analysis carried out 24–32 weeks after implantation. Because paraformaldehyde is a strong oxidizing agent, it was expected that dopamine remaining in the cylinder would be oxidized during the fixation procedure. In fact, a reddish-brown color was always observed in the trajectory of nanostructured silica–dopamine implants, but not in those of empty silica reservoirs, which appeared translucent. This may be interpreted as evidence that the nanostructured matrix material still contained dopamine after six or eight months. Indeed, in vitro studies have shown that dopamine molecules embedded in silica nanostructured material remain stable for a long time.[26]

Histologic analysis revealed that the silica nanostructured implants were always located in the lateral region of the striatum. In all cases, the implants containing dopamine showed a reddish-brown color, suggesting the presence of oxidized dopamine (Figures 18A and 18B), while implants without dopamine were always translucent (Figures 18C and 18D).

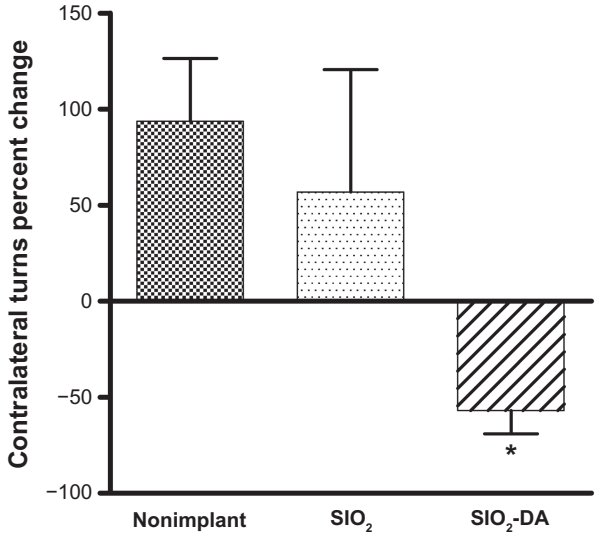

Figure 17 Percent change of circling behavior between the first and second apomorphine challenges. Note that only the silica–dopamine group showed a significant decrease in the number of turns compared with the nonimplanted group (Kruskal–Wallis test = 7.45; *$P < 0.05$ versus nonimplant, Dunn's test).

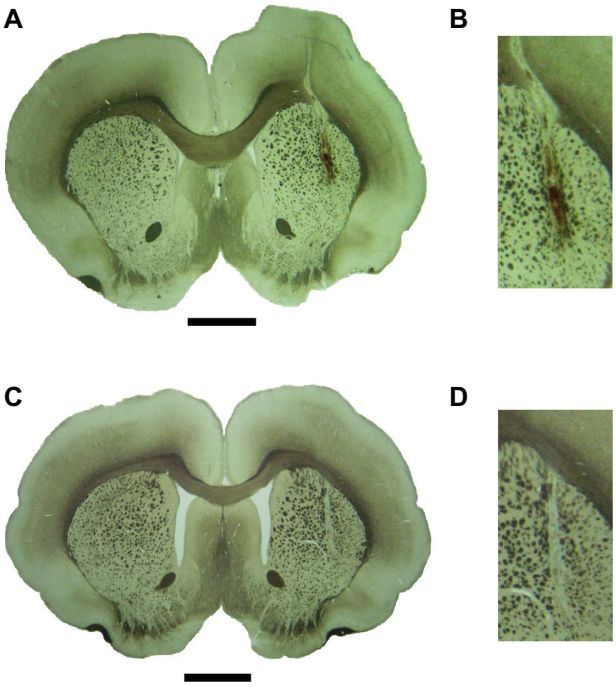

Figure 18 Coronal brain sections (50 μm) showing the site of intrastriatal implants. **A)** Freshly cut section of paraformaldehyde-fixed rat brain showing the trajectory of the dopamine-impregnated silica implant. Scale bar 2 mm. **B)** Higher magnification of the same silica–dopamine implant. Note the reddish-brown color characteristic of oxidized dopamine. **C)** Brain section from a rat implanted with the empty silica reservoir. Scale bar 2 mm. **D)** Higher magnification of the empty silica implant. Note the translucent color of the nanosilicon gel.

Conclusion

We developed amorphous nanostructured silica–dopamine materials with morphology consisting of aggregated particles and sizes that depend on the quantity of dopamine contained in them. Dopamine was stabilized into this morphology, forming weak hydrogen bonds with Si-OH groups of silica. The in vitro dopamine release profiles indicate the existence of two different release steps, a fast-sustained release during the first 24 hours and from then on a fixed slow rate of release.

The major finding of this study was that intrastriatal silica–dopamine implants in hemiparkinsonian rats reversed the rotational asymmetry induced by apomorphine, a dopamine agonist. In contrast, apomorphine-induced rotation increased in animals without an implant, and remained unchanged in animals implanted with an empty silica reservoir. The striatal area in which the implants were situated has been reported by others as a region related to motor modulation.[39] In rats implanted with the silica–dopamine nanomaterial, the number of apomorphine-induced rotations was reduced to 57% of preimplant values. This effect is similar to that observed after intrastriatal transplantation of dopaminergic embryonic cells, which reduce apomorphine-induced circling behavior by about 50% of pregrafting values, an effect which was attributed to sprouting of dopaminergic axons.[27]

It should be noted that rats implanted with silica–dopamine showed no signs of dyskinesias at any time, an observation which would be consistent with a slow and tonic dopamine release. This contrasts with the effect of intermittent systemic L-dopa administration, which causes orofacial dyskinesias. In summary, because the nanostructured silica material has been found to be biocompatible with cerebral tissue,[25] we may conclude that it has the potential to be used as a release system for dopamine in patients with Parkinson's disease.

Acknowledgments

We thank Angeles Miguel, Itzel Sánchez, M Martínez-Rosales, G Mendoza-Díaz, and León Albarrán for their technical assistance. The in vivo study was supported by grants UADY-PRIORI-06-011 (JLBG) and CONACYT-SEP-2004-C01-47763 (JLGA). The reservoir development studies were supported by CONACYT-FONCICYT-96095 and ICyTDF (PICDS08-12). We also acknowledge the Instituto Nacional de Neurología y Neurocirugía in México for supporting this research financially and technically.

Disclosure

The authors report no conflicts of interest in this work.

References

1. Parkinson J. *An Essay on the Shaking Palsy*. London, UK: Sherwood Neely and Jones; 1817.
2. Harding AE. Movement disorders. In: Walton J, editor. *Brain Diseases of the Nervous System*. New York, NY: Oxford University Press; 1993.
3. Guttman M, Kish SJ, Furukawa Y. Current concepts in the diagnosis and management of Parkinson's disease. *Can Med Assoc J*. 2003; 168:293–301.
4. Paulson GW, Dadmehr N. Is there a premorbid personality typical for Parkinson's disease? *Neurology*. 1991;41:73–76.
5. Menza MA, Golbe LI, Cody RA, Forman NE. Dopamine-related personality traits in Parkinson's disease. *Neurology*. 1993;43: 505–508.
6. Fujii C, Harada S, Ohkoshi N, Hayashi A, Yoshizawa K. Cross cultural traits for personality of patients with Parkinson's disease. *Am J Med Genet*. 2000;96:1–3.
7. Gibb WR, Lees AJ. A comparison of clinical and pathological features of young- and old-onset Parkinson's disease. *Neurology*. 1988; 38:1402–1406.
8. Goudreau JL, Ahlskog JE. Symptomatic treatment of Parkinson's disease: Levodopa. In: Ebadi M, Pfeiffer RF, editors. *Parkinson's Disease*. London: CRC Press; 2005.
9. Hely MA, Morris JG, Reid WG, O'Sullivan DJ, Williamson PM, Rail D. The Sydney multicentre study of Parkinson's disease: A randomised, prospective 5 years study comparing low dose bromocriptine with lowdose levodopa-carbidopa. *J Neurol Neurosurg Psychiatr*. 1994; 57:903–910.
10 Marsden CD, Parkes JD, Quinn N. Fluctuations in disability in Parkinson's disease – clinical aspects. In: Marsden CD, Fahn S, editors. *Movement Disorders*. London: Butterworths; 1981.
11. García-Escrig M, Bermejo-Pareja F. Complicaciones motoras del tratamiento con levodopa en la enfermedad de Parkinson. *Rev Neurol*. 1999;28:799–809.
12. Katzung BG. Pharmacological management of Parkinsonism and other movement disorders. In*: Basic and Clinical Pharmacology*. 8th ed. New York, NY: Lange Medical Books/McGraw Hill Companies Inc; 2001.
13. Cuenca AG, Jiang H, Hochwald SN, Delano M, Cance WG, Grobmyer SR. Emerging implications of nanotechnology on cancer diagnostics and therapeutics. *Cancer*. 2006;107:459–466.
14. Son SJ, Bai X, Lee SB. Inorganic hollow nanoparticles and nanotubes in nanomedicine Part 1. Drug/gene delivery applications. *Drug Discov Today*. 2007;12:650–656.
15. Desai MP, Labhasetwar V, Amidon GL, Levy RJ. Gastrointestinal uptake of biodegradable microparticles: Effect of particle size. *Pharm Res*. 1996;13:1838–1845.
16. Desai MP, Labhasetwar V, Walter E, Levy RJ, Amidon GL. The mechanism of uptake biodegradable microparticles in Caco-2 cells is size dependent. *Pharm. Res*. 1997;14:1568–1573.
17. Barbé C, Bartlett J, Kong L, et al. Silica particles: A novel drug-delivery system. *Adv Mater*. 2004;16:1959–1966.
18. Slowing I I, Vivero-Escoto J L, Wu ChW, Lin VSY. Mesoporous silica nanoparticles as controlled release drug delivery and gene transfection carriers. *Adv Drug Deliv Rev*. 2008;60:1278–1288.
19. Rosenholm JM, Lindén M. Toward establishing structure-activity relationships for mesoporous silica in drug delivery applications. *J Control Release*. 2008;128:157–164.
20. Hirvonen J. Feasibility of silicon and silica-based mesoporous materials for oral drug delivery applications. *Eur J Pharm Sci*. 2008;9 (34 Suppl):S1.

21. Viitala R, Jokinen M, Tuusa S, Rosenholm JB, Jalonen H. Adjustably bioresorbable sol-gel derived SiO_2 matrices for release of large biologically active molecules. *J Sol Gel Sci Technol*. 2005;36: 147–156.
22. Lopez T, Ortiz E, Quintana P, Gonzalez RD. A nanostructured titania bioceramic implantable device capable of drug delivery to the temporal lobe of the brain. *Colloids Surf A Physicochem Eng Asp*. 2007; 3003–3010.
23. López T, Asomoza M, Picquart M, et al. Study of the sodium phenytoin effect on the formation of sol-gel SiO_2 nanotubes by TEM. *Opt Mater*. 2005;27:1270–1275.
24. Avni DA, Coradin T, Lev O, Livage J. Recent bio-applications of sol-gel materials. *J Mater Chem*. 2006;16:1013–1030.
25. López T, Basaldella EI, Ojeda ML, Manjarrez J, Alexander-Katz R. Encapsulation of valproic acid and sodic phenytoin in ordered mesoporous SiO_2 solids for the treatment of temporal lobe epilepsy. *Opt Mater*. 2006;29:75–81.
26. López T, Quintana P, Martínez JM, Esquivel D. Stabilization of dopamine in nanosilica sol-gel matrix to be used as a controlled drug delivery system. *J Non-Cryst Solds*. 2007;353:987–989.
27. Nikkhah G, Duan WM, Knappe U, Jödicke A, Björklund A. Restoration of complex sensoriomotor behavior and skilled forelimb use by a modified nigral cell suspension transplantation approach in the rat Parkinson model. *Neuroscience*. 1993;56:33–43.
28. Lopez T, Sotelo J, Navarret J, Ascencio JA. Synthesis of TiO_2 nanostructured reservoir with temozolomide: Structural evolution of the occluded drug. *Opt Mater*. 2006;29:88.
29. Paxinos G, Watson W. *The Rat Brain in Stereotaxic Coordinates*. 2nd ed. San Diego, CA: Academic Press; 1986.
30. Heredia-López FJ, Bata-García JL, Álvarez-Cervera FJ, Góngora-Alfaro JL. A novel rotometer based on a RISC microcontroller. *Behav Res Methods Instrum Comput*. 2002;34:399–407.
31. Angel-Guío JE, Charris JE, Pérez J, et al. Synthesis and theoretical study of 2-amino-2,3,3a,4,5,6-hexahydro-1H-phenalene and its biological evaluation on central dopaminergic system. *Farmaco*. 2000;55: 575–582.
32. Aliste MP. Theoretical study of dopamine. Application of the HSAB principle to the study of drug-receptor interactions. *THEOCHEM*. 2000; 507:1–10.
33. Gregg SG, Sing SW. *Adsorption Surface Area and Porosity*. 2nd ed. New York, NY: Academic Press; 1982.
34. Barrett EP, Joyner LG, Halenda PJ. The determination of pore volume and area distribution in porous solids. I. Computations from nitrogen isotherms. *Am Chem Soc*. 1951;73:373–380.
35. Wood DL, Rabinovich EM. Study of alkoxide silica gels by infrared spectroscopy. *Appl Spectrosc*. 1989;43:263–267.
36. Ungerstedt U. Postsynaptic supersensitivity after 6-hydroxydopamine induced degeneration of the nigrostriatal dopamine system. *Acta Physiol Scand*. 1971;367:69–93.
37. Hefti F, Melamed E, Wurtman RJ. Partial lesions of the dopaminergic nigrostriatal system in rat brain: Biochemical characterization. *Brain Res*. 1980;195:123–137.
38. Bata-García JL, Villanueva-Toledo J, Gutiérrez-Ospina G, Alvarez-Cervera FJ, Heredia-López FJ, Góngora-Alfaro JL. Sustained improvement of motor function in hemiparkinsonian rats chronically treated with low doses of caffeine or trihexyphenidyl. *Pharmacol Biochem Behav*. 2007;86:68–78.
39. Chang JW, Wachtel SR, Young D, Kang UJ. Biochemical and anatomical characterization of forepaw adjusting steps in rat models of Parkinson's disease: Studies on medial forebrain bundle and striatal lesions. *Neuroscience*. 1999;88:617–628.